

Melnick 39 is a very massive intermediate-period colliding-wind binary

A. M. T. Pollock,¹★ P. A. Crowther,¹ J. M. Bestenlehner,¹ Patrick S. Broos² and Leisa K. Townsley²†

¹*Astrophysics Research Cluster, School of Mathematical and Physical Sciences, University of Sheffield, Hounsfield Road, Sheffield, S3 7RH, UK*

²*Department of Physics & Astronomy, 525 Davey Laboratory, Pennsylvania State University, University Park, PA 16802, USA*

Accepted 2025 March 20. Received 2025 March 20; in original form 2024 July 18

ABSTRACT

Individually identified binary systems of very massive stars define fixed points on possible evolutionary pathways that begin with extreme star formation and end in either coalescence of compact remnants or complete disruption as pair-production supernovae. The LMC star Melnick 39 in the Tarantula Nebula is revealed to be an eccentric ($e = 0.618 \pm 0.014$) binary system of reasonably long period from time-series analysis of *Chandra* T-ReX X-ray observations. Its X-ray luminosity scales with the inverse of the binary separation, as expected for colliding-wind binaries in the adiabatic regime. The inclusion of optical time-series spectroscopy from the VLT FLAMES Tarantula Survey and archival *HST* spectroscopy confirms Melnick 39 as a double-lined O2.5 If/WN6+O3 V–III spectroscopic binary with orbital period near 648 days. We obtain a mass ratio of $q = 0.76 \pm 0.06$, and minimum dynamical masses of 105 ± 11 and $80 \pm 11 M_{\odot}$ for the O2.5 If/WN6 and O3 V–III components, plus photometric evidence for an orbital inclination near 90° . Disentangled spectroscopy allows the physical and wind properties of the primary to be determined, including $T_{\ast} = 44$ kK, $\log L/L_{\odot} = 6.2$, $\log \dot{M}/M_{\odot} \text{ yr}^{-1} = -5.0$. Its dynamical mass agrees closely with $109 M_{\odot}$ obtained from the mass-luminosity relation of very massive stars.

Key words: stars: Wolf-Rayet – stars: massive – stars: winds, outflows – binaries: eclipsing – X-rays: stars – shock waves

1 INTRODUCTION

The detection of compact mergers by LIGO/Virgo gravitational wave observatories has led to renewed interest in massive binaries, especially within the low metallicity environments of the Magellanic Clouds, some of which may have been identified as candidate progenitors of black hole mergers (Belczynski et al. 2022). It is now established that the majority of massive stars are members of binary systems (Sana et al. 2012, 2013). Long-period systems can be identified via high spatial resolution imaging or interferometry, while short-period systems are preferentially detected through eclipses or spectroscopic campaigns (Moe & Di Stefano 2017).

X-ray monitoring offers one route to identifying the more observationally challenging intermediate period systems owing to X-ray variability arising from wind-wind collisions within eccentric orbits. The Tarantula Nebula hosts the richest massive stellar population within the Local Group (Crowther 2019) and has been observed with the *Chandra* X-ray Visional Project ‘The Tarantula - Resolved by X rays’ designated T-ReX (Townsley et al. 2024). Some of its X-ray light curves have indeed been used to identify candidate binary systems such as Melnick 34 (Pollock et al. 2018; Tehrani et al. 2019) and Melnick 33Na (Bestenlehner et al. 2022) subsequently confirmed as such.

Melnick 39¹ (Melnick 1985), hereafter Mk 39 (aka VFTS 482, Brey 78 or BAT99 99 notwithstanding some SIMBAD name con-

fusion) is an Of/WN star (Walborn & Blades 1997; Crowther & Walborn 2011), located at a projected distance of 3 pc NW of R136 at the heart of the Tarantula Nebula. Spectroscopic analysis of Mk 39 by Bestenlehner et al. (2014) revealed a very high bolometric luminosity ($\log L/L_{\odot} \sim 6.4$) and inferred stellar mass ($\sim 145 M_{\odot}$). Mk 39 is one of the brightest X-ray sources in the Tarantula Nebula (Portegies Zwart et al. 2002; Townsley et al. 2006). Crowther et al. (2022) analysed the cumulative T-ReX dataset to determine a mean $\log L_X/(\text{erg s}^{-1}) = 34.3$, while other tentative evidence for binarity has also been reported (Massey et al. 2002, 2005) including a preliminary orbital period of 92.6 ± 0.3 days from radial velocity variability (Schnurr et al. 2008). These collective characteristics are strongly suggestive of a colliding-wind binary system involving very massive components (Stevens et al. 1992).

Large samples of OB stars in the Tarantula Nebula were observed spectroscopically via the VLT/FLAMES Tarantula Survey (VFTS, Evans et al. 2011), which included Mk 39, although follow-up radial velocity studies have been focused on normal OB stars (Mahy et al. 2020; Villaseñor et al. 2021). In this paper we confirm the binary nature of Mk 39; establish its orbital period; and determine its component mass ratio from analysis of VFTS and archival *Hubble Space Telescope* (*HST*) spectroscopy.

2 ORBITAL PERIOD OF MK 39 FROM X-RAYS

The 2Ms *Chandra* T-ReX program (Townsley et al. 2024) was obtained over 630 days between 2014 May 3 and 2016 January 22 using the ACIS-I instrument centred on R136a, the central cluster of the Tarantula Nebula. For this study we incorporate 92 ks of ACIS

★ E-mail: A.M.Pollock@sheffield.ac.uk

† Published posthumously

¹ SIMBAD: "Cl* NGC 2070 MEL 39"

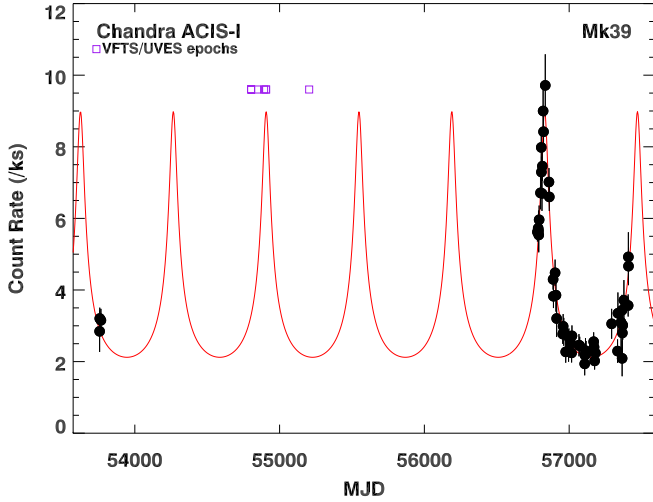


Figure 1. Least-squares fit of $1/D$ to *Chandra* ACIS-I T-ReX sensitivity-corrected count rates of Mk 39 supplemented by earlier ACIS-I data from 2006 (Townsley et al. 2014) implying $P = 641.1^{+4.3}_{-3.3}$ d, $e = 0.618 \pm 0.014$, $T_0 = 56830.6 \pm 1.4$ MJD. Also shown are the 7 epochs, some overlapping, of the VFTS optical spectroscopy reported in Table 2

Table 1. Keplerian orbital solution for Mk 39 from fits to the T-ReX X-ray light curve (Townsley et al. 2024) and to optical spectroscopy obtained in this study from VFTS (Evans et al. 2011) and *HST* (Massey et al. 2005).

Parameter	Result	Method
P	648.6 ± 0.9 d	VFTS, <i>HST</i>
T_0 (MJD)	56830.6 ± 1.4	<i>Chandra</i> T-ReX
e	0.618 ± 0.014	<i>Chandra</i> T-ReX
K_1	76.9 ± 4.3 km s $^{-1}$	VFTS, <i>HST</i>
K_2	101.4 ± 6.6 km s $^{-1}$	VFTS, <i>HST</i>
v_{sys}	260.5 ± 3.2 km s $^{-1}$	VFTS, <i>HST</i>
ω	$130.4 \pm 3.6^\circ$	VFTS, <i>HST</i>

observations from 2006 January 21–30 (Townsley et al. 2014). Data reduction, point-source detection and extraction are summarised in Crowther et al. (2022) who noted that Mk 39 is an X-ray variable. The X-ray luminosities of colliding-wind binaries in the adiabatic regime are expected to depend on the inverse of the binary separation, D , (e.g. Stevens et al. 1992) as observed closely to apply over most of the long-period eccentric orbit of WR 140 (Pollock et al. 2021). Fig. 1 provides a least-squares fit of $1/D$ to the full dataset, revealing an excellent match for an orbital period of $P = 641.1^{+4.3}_{-3.3}$ days, $e = 0.618 \pm 0.014$ and $T_0 = 56830.6 \pm 1.4$ MJD. The inferred orbital period narrowly exceeds the length of the 2014–2016 T-ReX campaign, which provides a strict lower limit to the period as the rising portion of the light curve at the end of the T-ReX campaign did not reach the level observed at the beginning. This also accounts for asymmetric errors in the period estimate. Critical in obtaining the solution were individual observation sensitivity corrections and inclusion of the measurements made in 2006. Details of the X-ray solution and an observation log are given in Appendix A.

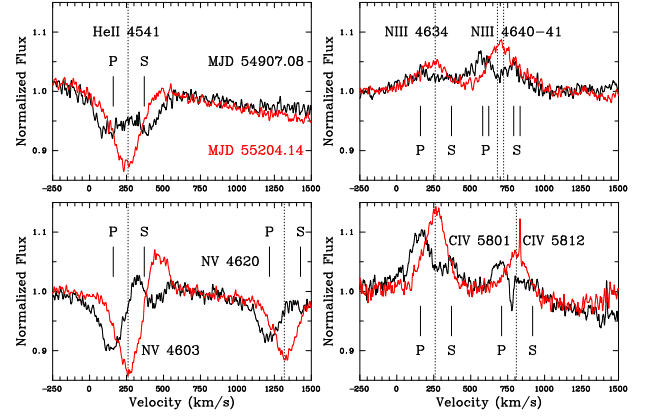


Figure 2. Observed VLT/UVES radial velocities of selected lines of Mk 39 (black: MJD 54907.08, red: MJD 55204.14) indicating primary (P) and secondary (S) components and systemic velocities (dotted lines)

3 OPTICAL ORBITAL SOLUTION FOR MK 39

In order to assess the reliability of the X-ray orbital solution of Mk 39 (VFTS 482) and establish the nature of the individual components we have taken advantage of archival spectroscopy acquired at 7 epochs via the VLT/FLAMES Tarantula Survey (Evans et al. 2011) between 2008 December 3 and 2010 January 8 (MJD 54803–55204) with the UV-Visual Echelle Spectrograph (UVES, D’Odorico et al. 2000). For each epoch two exposures of 1815 sec were obtained with the red arm using the $\lambda 520$ nm central wavelength, providing coverage between 4175–5155 Å and 5240–6200 Å at a spectral resolution of $R=53,000$.

UVES reveals spectroscopic variability of Mk 39, including double lines of He II $\lambda 4542$, 5412 from 2009 March 3–17 (MJD 54893–54907), as indicated in Fig. 2, fortuitously corresponding to what proves to be a quadrature phase near X-ray maximum (Fig. 1), supporting the X-ray orbital solution and establishing Mk 39 as a double-lined spectroscopic binary (SB2). He II $\lambda 4686$ is severely blended at all epochs, while the cores of the H β and H γ absorption lines are contaminated with strong nebular emission.

We have supplemented VLT/UVES spectroscopy of Mk 39 with the archival *HST*/FOS spectroscopy described by Massey et al. (2005) from 1997 January 1 (GO 6417, P.I. P. Massey) and *HST*/STIS spectroscopy from 1998 February 4 (GO 7739, P.I. P. Massey). The FOS dataset used the G400H grating, covering $\lambda\lambda 3235$ –4781 Å at $R \sim 1300$. The STIS dataset used the G430M/4451 setting, covering $\lambda\lambda 4310$ –4593 Å at $R \sim 6000$, while the G750M/6581 setting covers $\lambda\lambda 6297$ –6866 Å at $R \sim 5000$ and includes H α . These datasets greatly extend the He II $\lambda 4542$ spectroscopic baseline, and so help to constrain the orbital period of the system.

Mk 39 has received previous spectral classifications of O4 If (Melnick 1985), O3 If*/WN6 (Walborn & Blades 1997), O2 If* (Massey et al. 2005) and O2.5 If/WN6 (Crowther & Walborn 2011), the latter based on the UVES data used here. The primary is confirmed as an O2.5 If/WN6 star, since the morphology of H β is a clear P Cygni profile. The UVES observations close to periastron (Fig. 2) permit the spectral type of the secondary to be determined. From comparison with early-O templates (Walborn et al. 2002), He II $\lambda 4542$, 5412 are strong, with He I $\lambda 4471$ weak or absent, plus weak N V $\lambda 4603$ –20

Table 2. Radial velocities in km s^{-1} of spectral features in the primary and secondary components of Mk 39 from VLT/UVES spectroscopy. Epochs correspond to the midpoints of observations.

MJD	He II $\lambda 4542$		N V $\lambda 4603$	N III $\lambda 4641$	He II $\lambda 5412$		C IV $\lambda 5801$
	Primary	Secondary	Primary	Primary	Primary	Secondary	Primary
54803.17	290.9 $^{+3.0}_{-3.3}$	210.1 $^{+3.2}_{-3.4}$	299.2 $^{+3.9}_{-3.8}$	248.7 $^{+5.1}_{-5.1}$	305.0 $^{+3.9}_{-4.0}$	188.3 $^{+3.8}_{-4.1}$	291.7 $^{+4.6}_{-4.7}$
54803.22	292.3 $^{+2.8}_{-2.8}$	205.1 $^{+2.5}_{-3.8}$	300.7 $^{+3.7}_{-3.7}$	240.4 $^{+4.1}_{-4.2}$	301.1 $^{+3.6}_{-3.6}$	185.4 $^{+3.6}_{-3.6}$	290.5 $^{+4.5}_{-4.5}$
54851.10	295.1 $^{+2.2}_{-4.3}$	215.9 $^{+4.4}_{-4.2}$	283.3 $^{+3.5}_{-3.5}$	238.3 $^{+5.3}_{-5.3}$	314.5 $^{+3.6}_{-3.6}$	182.8 $^{+4.0}_{-3.6}$	282.5 $^{+4.7}_{-4.7}$
54893.04	105.9 $^{+4.8}_{-4.1}$	401.7 $^{+3.8}_{-3.8}$	157.8 $^{+3.9}_{-3.9}$	95.5 $^{+7.0}_{-7.0}$	114.1 $^{+4.5}_{-4.2}$	398.4 $^{+5.6}_{-5.1}$	171.0 $^{+4.7}_{-4.2}$
54906.01	152.6 $^{+3.4}_{-3.9}$	379.6 $^{+7.4}_{-7.2}$	186.1 $^{+4.8}_{-4.8}$	133.8 $^{+9.0}_{-9.1}$	113.4 $^{+5.7}_{-5.6}$	378.3 $^{+5.8}_{-5.8}$	187.2 $^{+5.6}_{-5.8}$
54907.08	132.6 $^{+4.8}_{-4.7}$	396.4 $^{+5.9}_{-4.2}$	177.9 $^{+3.3}_{-3.3}$	135.1 $^{+4.7}_{-4.7}$	138.4 $^{+3.8}_{-3.7}$	364.8 $^{+4.2}_{-4.2}$	198.3 $^{+4.5}_{-4.5}$
55204.14	294.2 $^{+3.2}_{-3.0}$	215.7 $^{+3.8}_{-3.9}$	297.1 $^{+3.7}_{-3.7}$	253.9 $^{+4.1}_{-4.1}$	298.5 $^{+3.2}_{-3.0}$	195.3 $^{+3.8}_{-3.9}$	293.2 $^{+4.4}_{-4.4}$

absorption and N III $\lambda\lambda 4634-41$ emission, implying O3 V-III for the secondary.

We have undertaken single or double gaussian fits to various optical absorption lines in VLT/UVES spectra to establish the individual component radial velocities presented in Table 2. In addition, we have used a grid of CMFGEN model atmospheres (Hillier & Miller 1998) suitable for early-type O stars of LMC metallicity (Bestenlehner et al. 2014) to cross correlate with VLT/UVES and HST/FOS+STIS spectroscopy. Radial velocities of the primary and secondary components are presented in Table 3, having been derived by investigating the extrema and zero-points of the second and third derivatives of the cross-correlation function.

To derive the orbital parameters we have used these uncertainty weighted averages and employed the MCMC approach of Tehrani et al. (2019). As the VLT/UVES data provide poor orbital phase coverage, we fixed the eccentricity to the X-ray photometric solution from Section 2 and utilised $T_0 = 56830.6 \pm 1.4$ MJD as a prior. We obtained the solution reported in Table 1 and illustrated in Figure 3 with period $P = 648.6 \pm 0.9$ d, leading to minimum masses $M_1 \sin^3 i = 105 \pm 11 M_\odot$ and $M_2 \sin^3 i = 80 \pm 11 M_\odot$ and mass ratio $q = K_1/K_2 = M_2/M_1 = 0.76 \pm 0.06$. The systemic velocity $v_{\text{sys}} = 260 \pm 3 \text{ km s}^{-1}$ of Mk 39 is close to the mean radial velocity of $268 \pm 6 \text{ km s}^{-1}$ of OB stars within 5 pc of R136 (Hénault-Brunet et al. 2012).

The X-ray and optical period estimates differ by between 1 and 2σ due to larger positive errors in the X-ray value with any inconsistency probably reflecting systematic errors of which no account has been taken. Appendix A below discusses some of these in the X-ray 1/D regime. In the optical, the solution is quite well constrained by the appearance of double lines in 3 epochs over an interval of 14 days with the closest of the 4 epochs in which the double lines were not resolved in a key observation 42 days earlier. An alternative solution to that reported in Table 1 is available by exchanging primary and secondary radial velocities in that key observation at MJD 54851.10. Although this is formally superior in statistical terms, the implied period of $P = 653.2 \pm 0.4$ d is less consistent with the X-ray value. These uncertainties should be eliminated by future suitably well-timed observations in either X-ray photometry or optical spectroscopy around periastron the next of which is expected to occur in late 2026.

4 PHYSICAL AND WIND PROPERTIES OF MK 39

Armed with the orbital solution of Mk 39 from the previous section, we have disentangled the components of the UVES spectroscopy following the approach of Bestenlehner et al. (2022) for the SB2 system Mk 33Na, which includes rescaling according to the flux ratio of the individual components. For the physical and wind properties

Table 3. Radial velocities in km s^{-1} of primary and secondary components of Mk 39 from cross-correlation of VLT/UVES and HST/FOS+STIS spectroscopy. Epochs correspond to the midpoints of observations.

MJD	Dataset	Primary	Secondary
50449.89	HST/FOS	183 \pm 10	336 \pm 10
50848.83	HST/STIS	309 \pm 10	205 \pm 10
54803.17	VLT/UVES	315 \pm 7	195 \pm 7
54803.22	VLT/UVES	315 \pm 7	196 \pm 7
54851.10	VLT/UVES	303 \pm 7	225 \pm 7
54893.04	VLT/UVES	125 \pm 6	393 \pm 5
54906.01	VLT/UVES	140 \pm 6	366 \pm 5
54907.08	VLT/UVES	147 \pm 5	361 \pm 5
55204.14	VLT/UVES	288 \pm 9	226 \pm 8

of the individual components of Mk 39. Bestenlehner et al. (2014) obtained a system luminosity of $\log L/L_\odot = 6.4$ that we adopt here ($E(B - V) = 0.45$, $R_V = 3.26$), together with the mass ratio $q = 0.76$. For LMC very massive main sequence stars $L \propto M^{1.4 \pm 0.2}$ (Köhler et al. 2015), so $L_2/L_1 \sim 0.7$ and $\log(L_1/L_\odot) = 6.2$ and $\log(L_2/L_\odot) = 6.0$.

Comparisons between disentangled UVES spectra (blue) and synthetic CMFGEN spectra (red) for each component are presented in Fig. 4 with the STIS H α region in Fig. 5. Disentangled secondary spectra at H γ and He II $\lambda 4686$ are unreliable owing to the dominant primary spectral lines as well as nebular Balmer-line contamination. We obtain stellar temperatures of $T_* = 44.0 \pm 2.5$ kK and 48.0 ± 2.5 kK respectively for the primary and secondary from N V $\lambda\lambda 4603-20$ and He II $\lambda 4542/5411$ since He I $\lambda 4471$, $\lambda 5876$ are dominated by nebular emission. N IV $\lambda 4058$ is not included in the UVES data, so use of solely nitrogen diagnostics would rely on the N V doublet and N III $\lambda 4634-41$, requiring a lower temperature for the primary and higher temperature for the secondary, subject to uncertainties in their nitrogen abundances. Weak emission in the C IV $\lambda\lambda 5801-12$ doublet is seen in both components, and is reasonably well reproduced for our preferred stellar temperatures.

We favour a mass-loss rate of about $10^{-5} M_\odot \text{ yr}^{-1}$ for the primary from He II $\lambda 4686$, supported by the morphology of H β and the STIS H α spectroscopy, whereas $10^{-6.2} M_\odot \text{ yr}^{-1}$ is estimated for the secondary owing to an absence of any suitable wind diagnostics. A wind velocity of 2600 km s^{-1} is adopted for both components following Bestenlehner et al. (2014) who analysed archival far-UV STIS/G140L spectroscopy of Mk 39 from Massey et al. (2005). We estimate equatorial rotational velocities $v_{\text{eq}} \sin i \sim 100 \text{ km s}^{-1}$ and 80 km s^{-1} from He II $\lambda 4542$, 5412 lines.

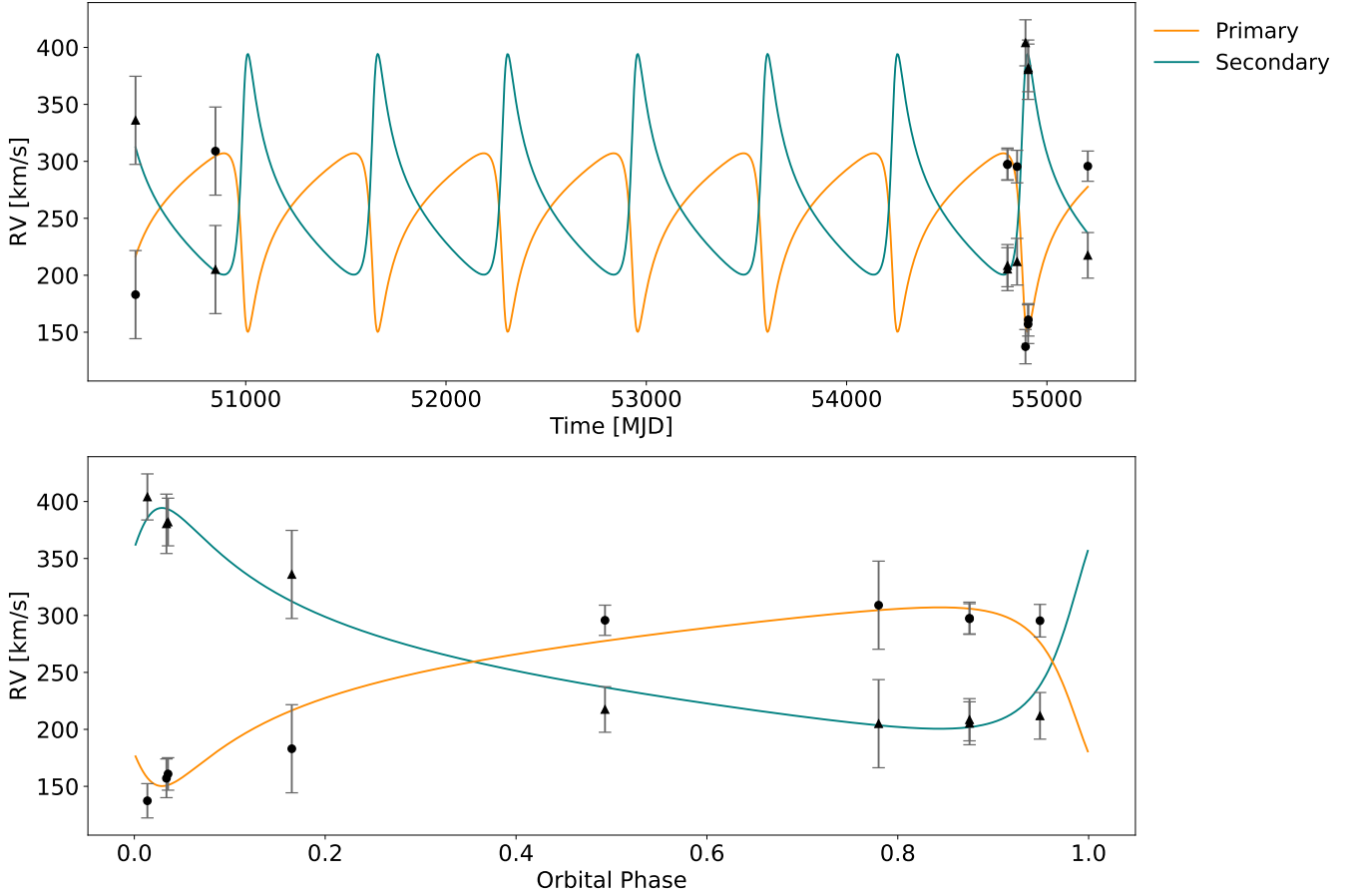


Figure 3. Orbital solution to He II $\lambda 4542$ VLT (UVES) and *HST* (FOS+STIS) radial velocities for the primary (filled circles) and secondary (filled triangles) components of Mk 39, revealing $K_1 = 76.9 \text{ km s}^{-1}$ and $K_2 = 101.4 \text{ km s}^{-1}$, $v_{\text{sys}} = 260 \pm 3 \text{ km s}^{-1}$, $P = 648.6 \pm 0.9$ days for $e = 0.618$ obtained from X-ray light curve fit, implying a mass ratio of $q = 0.76 \pm 0.06$.

High-resolution far ultraviolet spectroscopy of Mk 39 has been obtained via the *HST* ULLYSES survey of massive stars in the Magellanic Clouds (Roman-Duval et al. 2020), using COS G130M/1291 and G160M/1611, providing spectral coverage between $\lambda\lambda 1131$ –1790 at a spectral resolution of $R \sim 15,000$. These datasets were not used for our analysis, but the synthetic spectra provide a good match to O v $\lambda 1371$, Si iv $\lambda\lambda 1393$ –1402, He II $\lambda 1640$ and N iv $\lambda 1718$, while P Cygni emission for C iv $\lambda\lambda 1548$ –51 and N v $\lambda\lambda 1238$ –42 is underestimated, the latter mitigated by strong Ly α interstellar absorption and its sensitivity to X-ray production (excluded from our spectroscopic analysis). The reddened spectral energy distribution of Mk 39 provides a good match to COS far-UV, plus more recent STIS near-UV (G230LB) and blue visual (G430L) spectroscopy (GO 16230, P.I. D Massa).

BONNSAI² (Schneider et al. 2014) coupled to evolutionary models from Köhler et al. (2015) and empirical initial rotation velocities of Ramírez-Agudelo et al. (2013) infers stellar masses and ages of $M_{\text{evol}} = 83^{+20}_{-18} M_{\odot}$ and $69^{+14}_{-11} M_{\odot}$ and 1.5 ± 0.3 Myr and $1.1^{+0.3}_{-0.8}$ Myr for the primary and secondary, assuming the stars have evolved independently to date. These evolutionary mass estimates are somewhat lower than minimum dynamical mass determinations (BONNSAI

Table 4. Physical properties of the primary and secondary components of Mk 39 from the present study.

Property	Primary	Secondary	Reference
Spectral Type	O2.5 If/WN6	O3 V-III	This study
T_{eff} (kK)	44 ± 2.5	48 ± 2.5	This study
$\log(L/L_{\odot})$	6.20 ± 0.15	6.00 ± 0.15	This study
$\log \dot{M}/M_{\odot} \text{ yr}^{-1}$	-5.0 ± 0.2	$-6.2^{+0.2}_{-0.5}$	This study
v_{∞} (km s ⁻¹)	2600	2600:	Bestenlehner et al. (2014)
Y	0.30 ± 0.05	0.27 ± 0.05	This study
$v_{\text{eq}} \sin i$ (km s ⁻¹)	100	80	This study
$M_{\text{dyn}} \sin i$ (M_{\odot})	105.2	79.8	This study
M (M_{\odot})	109 ± 7	83 ± 5	Gräfener et al. (2011)
M_{evol} (M_{\odot})	83^{+20}_{-18}	69^{+14}_{-11}	BONNSAI
τ (Myr)	1.5 ± 0.3	$1.1^{+0.3}_{-0.8}$	BONNSAI

underpredicts stellar luminosities by 0.1 dex). The favoured age is consequently ~ 1.4 Myr, similar to the nearby massive star cluster R136 (Crowther et al. 2016; Brands et al. 2022). Alternatively, $M \sim 109 \pm 7 M_{\odot}$ and $83 \pm 5 M_{\odot}$ are obtained for the primary and secondary from the mass-luminosity relationship for very massive stars (Gräfener et al. 2011), suggesting an inclination close to $i = 90^{\circ}$.

Massey et al. (2002, their Fig. 5) reported a short-lived ~ 0.1

² The BONNSAI web-service is available at www.astro.uni-bonn.de/stars/bonnsai

magnitude photometric dip in the optical light curve of Mk 39 (alias HSH 7, [Hunter et al. 1995](#)) at MJD 51635.36–51. Our preferred orbital solution in Table 1 would suggest a conjunction with the primary in front at MJD 51627.5 \pm 7.5 with most of the uncertainty due to the orbital timing of period and periastron passage rather than the orbital geometry of eccentricity and longitude of periastron. Thus a period shorter within the error budget by 1.0 d would bring consistency between the orbital solution and the occurrence of a photometric dip due to a physical or wind eclipse that is clearly subject to confirmation to reinforce the suggestion of a high orbital inclination.

5 DISCUSSION AND CONCLUSIONS

We have established that the X-ray luminous Of/WN star Mk 39 in the Tarantula nebula is an SB2 colliding-wind binary with period of 648.6 \pm 0.9 days that follows the inverse separation law for adiabatic emission. In this respect, Mk 39 represents an ideal example with little or none of the deviations from adiabatic behaviour seen in other systems near periastron due, for example, to competitive cooling seen in WR 140 ([Pollock et al. 2021](#)); circumstellar absorption in WR 25, another very massive binary system ([Pradhan et al. 2021](#)); or perhaps a combination of both in Mk 34 and WR 21a ([Pollock et al. 2018](#)).

Mk 39, which reaches a maximum count rate near 10 cts/ks at the minimum periastron orbital separation of 3.5 AU according to the new orbital solution, may be compared with Mk 34, the brightest T-ReX colliding-wind binary at its minimum near 35 cts/ks ([Pollock et al. 2018](#)) at the similar but slightly larger separation maximum of 4.1 AU reached at apastron ([Tehrani et al. 2019](#)). This difference is roughly consistent with expectations of scaling laws ([Luo et al. 1990](#); [Stevens et al. 1992](#)) which may be recast from mass-loss rate and terminal velocity to use luminosity and velocity FWHM, Δv , of the He II $\lambda 4686$ wind line ([Crowther et al. 2023](#)) to suggest $L_X \propto (L\Delta v^{-3.2})_{\text{HeII}}$: X-rays from the weaker, faster wind of Mk 39 fall a factor of a few short of the stronger, slower wind of Mk 34.

Optical spectroscopy has been used to determine a mass ratio of $q = 0.76 \pm 0.06$, and minimum component masses of $105 \pm 11 M_\odot$ (O2.5 If/WN6) and $80 \pm 11 M_\odot$ (O3 V–III). These agree closely with masses from the [Gräfenr et al. \(2011\)](#) mass-luminosity relation for very massive stars based on physical properties determined from disentangled UVES spectroscopy, for an inclination close to 90°. The inability of [Massey et al. \(2005\)](#) to obtain a satisfactory spectroscopic fit for Mk 39 was attributed to its composite nature though [Bestenlehner et al. \(2014\)](#) obtained physical and wind properties of Mk 39 from VLT/UVES spectroscopy ([Evans et al. 2011](#)), supplemented by HST/STIS G140L and H α spectroscopy ([Massey et al. 2005](#)) plus K-band VLT/SINFONI spectroscopy.

The only previously published orbital solution was from [Schnurr et al. \(2008\)](#) who obtained $P = 92.6 \pm 0.3$ days, $K_1 = 91 \pm 19$ km s $^{-1}$ and $v_{\text{sys}} = 337 \pm 16$ km s $^{-1}$ from spectroscopic observations of He II $\lambda 4686$, assuming – with explicit caution – a circular orbit. Although narrower photospheric absorption lines, such as He II $\lambda 4542$ used in this study, are more straightforward diagnostics of Keplerian orbital motion than broader, slightly irregular, wind emission lines such as He II $\lambda 4686$ used by [Schnurr et al. \(2008\)](#), the radial velocities of this emission line in the current VLT/UVES data follow reasonably closely the primary’s absorption lines at roughly the same positive displacement of about 80 km s $^{-1}$. The inconsistency with the new orbital solution must lie elsewhere. According to the new ephemeris, it is plausible that the minimum and maximum radial velocity excursions that drive the earlier orbital solution coincide with quadratures near a projected periastron passage of the new eccentric solution on

2002 January 16 during the first season of observations, with the second season encompassing the subsequent apastron. However, this possibility fails because the maximum and minimum obtained during successive runs 20 days apart in 2001 December are too close together in time and too far apart in velocity to be consistent with the parameters in Table 1.

[Bestenlehner et al. \(2022, their table 5\)](#) provide a summary of massive binaries in the LMC. Of these, the most extreme systems are exclusive to the Tarantula Nebula: Mk 34 (WN5h+WN5h, [Tehrani et al. 2019](#)), R144 (WN5–6h+WN6–7h, [Shenar et al. 2021](#)), R139 (O6.5 Iafc+O6 Iaf, [Mahy et al. 2020](#)) and Mk 33Na (OC2.5 If+O4V, [Bestenlehner et al. 2022](#)) with eccentric orbits in the range 18–155 days, and primary masses comfortably exceeding the previous LMC record holder ([Massey et al. 2002](#)).

Mk 39 has similar stellar components, albeit with a significantly longer period orbit, as indicated in Fig. 6 which shows a cumulative distribution of OB orbital periods for the Tarantula Nebula from [Almeida et al. \(2017\)](#), supplemented by T-ReX results. X-ray photometric surveys can help facilitate an improved characterisation of orbital periods, eccentricities and mass ratios of massive stars in the LMC, together with continuing spectroscopic surveys ([Mahy et al. 2020](#); [Villaseñor et al. 2021](#)) at longer wavelengths.

ACKNOWLEDGEMENTS

This is part of a collection of papers publishing posthumously the unfinished work of LWK, the principal investigator of T-ReX. This work was supported by the Chandra X-ray Observatory General Observer grants GO5-6080X (PI: L. Townsley) and by GO4-15131X (PI: L. Townsley) and by the Penn State ACIS Instrument Team Contract SV4-74108. All of these were issued by the Chandra X-ray Center, which is operated by the Smithsonian Astrophysical Observatory for and on behalf of NASA under contract NAS8-03060. Based in part on observations obtained with the NASA/ESA Hubble Space Telescope, retrieved from the Mikulski Archive for Space Telescopes (MAST) at the STScI. STScI is operated by the Association of Universities for Research in Astronomy, Inc. under NASA contract NAS 5-26555. PAC and JMB are supported by the Science and Technology Facilities Council research grant ST/V000853/1 (PI: V. Dhillon).

DATA AVAILABILITY

All the observational data used in this article are freely available as follows: the X-ray data through the Chandra Data Archive at <https://cxc.cfa.harvard.edu/cda/>; the optical VLT/FLAMES spectra through the ESO Archive Science Portal at <https://archive.eso.org/scienceportal/home>; and the optical HST data through the Mikulski Archive for Space Telescopes at <https://mast.stsci.edu/portal/Mashup/Clients/Mast/Portal.html>. The synthetic CMFGEN model atmospheres of the primary and secondary stars are available on request.

REFERENCES

- Almeida L. A., et al., 2017, *A&A*, 598, A84
- Belczynski K., et al., 2022, *ApJ*, 925, 69
- Bestenlehner J. M., et al., 2014, *A&A*, 570, A38
- Bestenlehner J. M., Crowther P. A., Broos P. S., Pollock A. M. T., Townsley L. K., 2022, *MNRAS*, 510, 6133

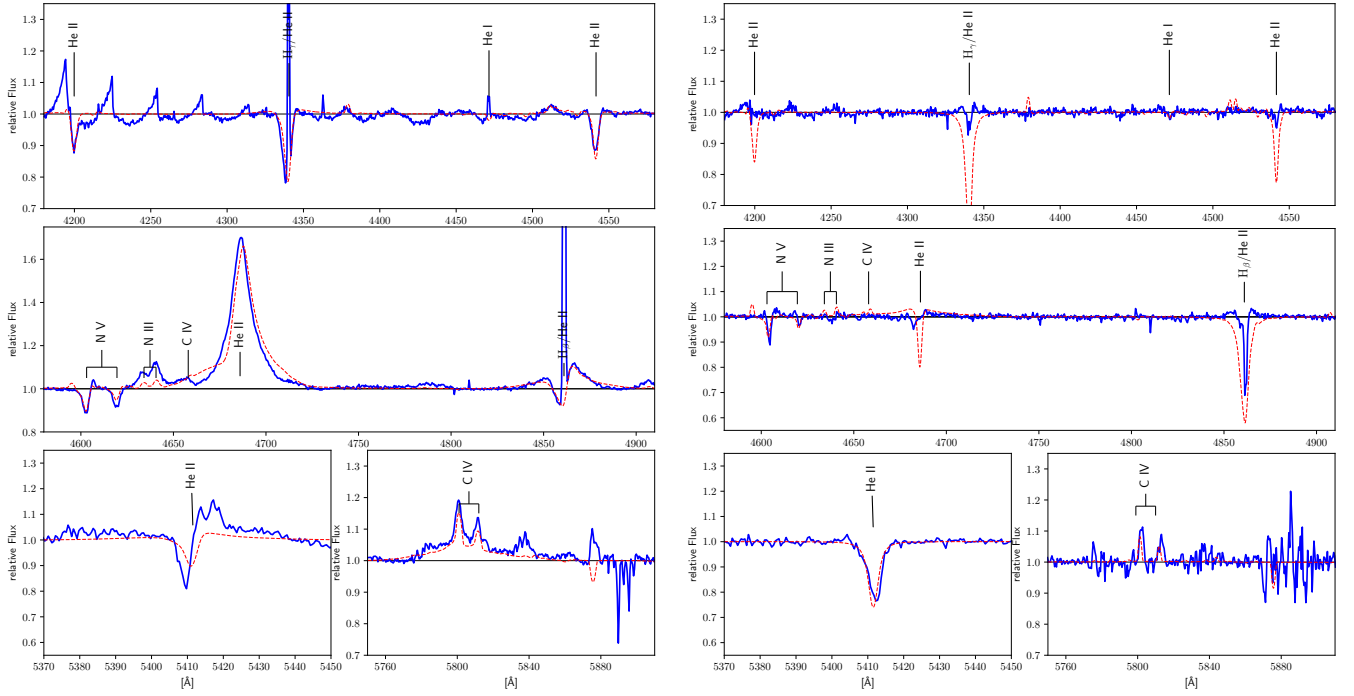


Figure 4. Comparison between disentangled Mk 39 primary (left) and secondary (right) UVES spectroscopy (blue solid lines) and synthetic CMFGEN spectra (red dotted lines). Strong nebular lines (Balmer, He I and [O III]) are present in the left panel, together with instrumental emission features shortward of 44300.

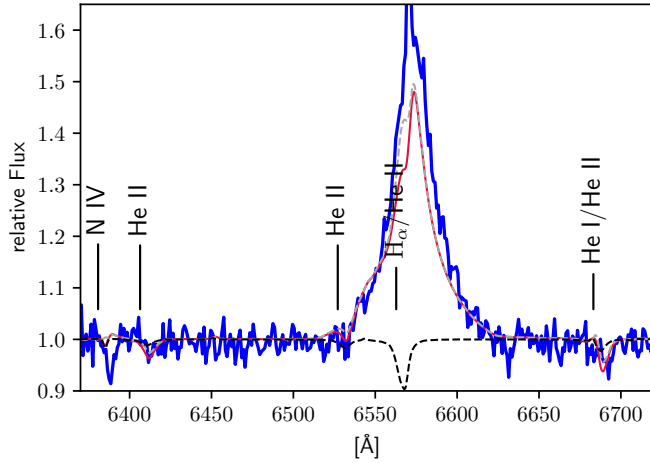


Figure 5. HST/STIS spectroscopy of Mk 39 near $H\alpha$ (solid blue) arising from a combination of dominant primary emission and weak secondary absorption.

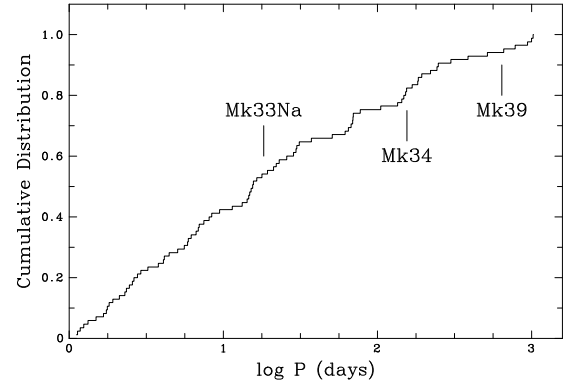


Figure 6. Cumulative distribution of orbital periods of OB stars in the Tarantula Nebula from Almeida et al. (2017) supplemented with T-ReX SB2 systems, Mk 34 (Tehrani et al. 2019), Mk 33Na (Bestenlehner et al. 2022) and Mk 39 from the present study with some long-period binaries are subject to revision.

- Brands S. A., et al., 2022, *A&A*, **663**, A36
 Crowther P. A., 2019, *Galaxies*, **7**, 88
 Crowther P. A., Walborn N. R., 2011, *MNRAS*, **416**, 1311
 Crowther P. A., et al., 2016, *MNRAS*, **458**, 624
 Crowther P. A., Broos P. S., Townsley L. K., Pollock A. M. T., Tehrani K. A., Gagné M., 2022, *MNRAS*, **515**, 4130
 Crowther P. A., Rate G., Bestenlehner J. M., 2023, *MNRAS*, **521**, 585
 D’Odorico S., Cristiani S., Dekker H., Hill V., Kaufer A., Kim T., Primas F., 2000, in Bergeron J., ed., *Society of Photo-Optical Instrumentation Engineers (SPIE) Conference Series Vol. 4005, Discoveries and Research Prospects from 8- to 10-Meter-Class Telescopes*. pp 121–130, doi:10.1117/12.390133
 Evans C. J., et al., 2011, *A&A*, **530**, A108

- Gräfener G., Vink J. S., de Koter A., Langer N., 2011, *A&A*, **535**, A56
 Hénault-Brunet V., et al., 2012, *A&A*, **546**, A73
 Hillier D. J., Miller D. L., 1998, *ApJ*, **496**, 407
 Hunter D. A., Shaya E. J., Holtzman J. A., Light R. M., O’Neil Jr. E. J., Lynds R., 1995, *ApJ*, **448**, 179
 Köhler K., et al., 2015, *A&A*, **573**, A71
 Luo D., McCray R., Mac Low M.-M., 1990, *ApJ*, **362**, 267
 Mahy L., et al., 2020, *A&A*, **634**, A118
 Massey P., Penny L. R., Vukovich J., 2002, *ApJ*, **565**, 982
 Massey P., Puls J., Pauldrach A. W. A., Bresolin F., Kudritzki R. P., Simon

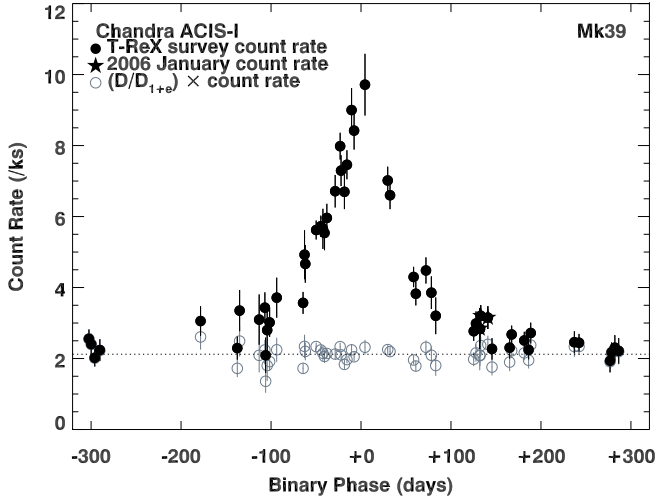


Figure A1. The X-ray orbit of Mk 39 with $P = 641.1$ d and $T_0 = 56830.6$ MJD with observed T-ReX count rates in solid black and the same values adjusted for the implied inverse binary separation shown in open grey.

periastron and in the less well sampled data after. Defects appear to be largely absent that could have been due to a variety of potential instrumental or physical causes such as uncertainties in the often substantial count-rate corrections shown in the table or the effects of absorption through stellar winds close to conjunctions.

For the purposes of predicting timing of future observations at or near periastron, in addition to the most accurately determined period of $P = 648.6 \pm 0.9$ d from the radial velocity analysis, it would be worth keeping in mind $P = 648.3 \pm 0.9$ d from the weighted mean of optical and X-ray values and $P = 647.6 \pm 1.4$ d from alignment of the putative photometric eclipse discussed in section 4.

This paper has been typeset from a \LaTeX file prepared by the author.

T., 2005, *ApJ*, 627, 477
Melnick J., 1985, *A&A*, 153, 235
Moe M., Di Stefano R., 2017, *ApJS*, 230, 15
Pollock A. M. T., Crowther P. A., Tehrani K., Broos P. S., Townsley L. K., 2018, *MNRAS*, 474, 3228
Pollock A. M. T., et al., 2021, *ApJ*, 923, 191
Portegies Zwart S. F., Pooley D., Lewin W. H. G., 2002, *ApJ*, 574, 762
Pradhan P., Huenemoerder D. P., Ignace R., Pollock A. M. T., Nichols J. S., 2021, *ApJ*, 915, 114
Ramírez-Agudelo O. H., et al., 2013, *A&A*, 560, A29
Roman-Duval J., et al., 2020, *Research Notes of the American Astronomical Society*, 4, 205
Sana H., et al., 2012, *Science*, 337, 444
Sana H., et al., 2013, *A&A*, 550, A107
Schneider F. R. N., Langer N., de Koter A., Brott I., Izzard R. G., Lau H. H. B., 2014, *A&A*, 570, A66
Schnurr O., Moffat A. F. J., St-Louis N., Morrell N. I., Guerrero M. A., 2008, *MNRAS*, 389, 806
Shenar T., et al., 2021, *A&A*, 650, A147
Stevens I. R., Blondin J. M., Pollock A. M. T., 1992, *ApJ*, 386, 265
Tehrani K. A., Crowther P. A., Bestenlehner J. M., Littlefair S. P., Pollock A. M. T., Parker R. J., Schnurr O., 2019, *MNRAS*, 484, 2692
Townsley L. K., Broos P. S., Feigelson E. D., Garmire G. P., Getman K. V., 2006, *AJ*, 131, 2164
Townsley L. K., Broos P. S., Garmire G. P., Bouwman J., Povich M. S., Feigelson E. D., Getman K. V., Kuhn M. A., 2014, *ApJS*, 213, 1
Townsley L. K., Broos P. S., Povich M. S., 2024, *ApJS*, 273, 5
Villaseñor J. I., et al., 2021, *MNRAS*, 507, 5348
Walborn N. R., Blades J. C., 1997, *ApJS*, 112, 457
Walborn N. R., et al., 2002, *AJ*, 123, 2754

APPENDIX A: THE X-RAY ORBITAL SOLUTION

Figure A1 shows the folded X-ray light curve resulting from the $1/D$ model of the observed T-ReX count rates logged in Table A1. Shown in grey are the observed count rate values scaled by the inverse ratio of the implied binary separation to the maximum separation at apastron, D_{1+e} . In a successful model, this quantity would be independent of phase. In this case, the observed dynamic range of about a factor of 5 is reproduced to within a few percent both before

Table A1. Binary-phase-ordered log of Chandra observations in the T-ReX survey of 30 Doradus and three earlier observations with observation ID and epoch; exposure time, T; sensitivity factor relative to the ObsID 7264 maximum; sensitivity-corrected count rate per 1000s of Mk 39; and phase interval covered, ϕ , of the 641.1-day best-fit X-ray orbit centred on MJD 56830.6.

ObsID	date	MJD	T(s)	factor	Mk 39 (cts/ks)	$\phi_{641.1}$ (d)
16445	2015-05-27T00:18:12	57169.013	49310	0.940	2.6 ± 0.3	-302.4 ± 0.3
17660	2015-05-29T14:55:28	57171.622	38956	0.941	2.4 ± 0.3	-299.9 ± 0.2
16446	2015-06-02T11:50:14	57175.493	47547	0.940	2.0 ± 0.2	-295.9 ± 0.3
17642	2015-06-08T05:11:14	57181.216	34438	0.915	2.2 ± 0.3	-290.3 ± 0.2
16449	2015-09-28T05:35:14	57293.233	24628	0.929	3.1 ± 0.4	-178.3 ± 0.2
18672	2015-11-08T01:04:22	57334.045	30574	0.928	2.3 ± 0.3	-137.5 ± 0.2
18706	2015-11-10T17:09:59	57336.715	14776	0.925	3.3 ± 0.6	-134.9 ± 0.1
18720	2015-12-02T10:49:02	57358.451	9832	0.928	3.1 ± 0.7	-113.2 ± 0.1
18721	2015-12-08T17:13:14	57364.718	25598	0.926	3.4 ± 0.4	-106.8 ± 0.2
17603	2015-12-09T15:27:36	57365.644	13778	0.929	2.1 ± 0.5	-106.0 ± 0.1
18722	2015-12-11T09:09:39	57367.382	9826	0.929	2.8 ± 0.7	-104.3 ± 0.1
18671	2015-12-13T23:41:12	57369.987	25617	0.927	3.0 ± 0.4	-101.6 ± 0.2
18729	2015-12-21T22:10:30	57377.924	16742	0.929	3.7 ± 0.6	-93.7 ± 0.1
18750	2016-01-20T00:41:30	57407.029	48318	0.926	3.6 ± 0.3	-64.4 ± 0.3
18670	2016-01-21T20:59:37	57408.875	14565	0.928	4.9 ± 0.7	-62.8 ± 0.1
18749	2016-01-22T16:14:19	57409.677	22153	0.926	4.7 ± 0.5	-61.9 ± 0.1
16192	2014-05-03T04:10:27	56780.174	93761	0.932	5.6 ± 0.3	-49.9 ± 0.6
16193	2014-05-08T10:15:25	56785.427	75994	0.929	5.7 ± 0.3	-44.7 ± 0.5
16612	2014-05-11T02:15:31	56788.094	22672	0.955	5.7 ± 0.6	-42.3 ± 0.2
16194	2014-05-12T20:00:24	56789.834	31333	0.898	5.5 ± 0.5	-40.6 ± 0.2
16615	2014-05-15T08:24:45	56792.351	45170	0.954	6.0 ± 0.4	-38.0 ± 0.3
16195	2014-05-24T14:09:28	56801.590	44405	0.827	6.7 ± 0.5	-28.7 ± 0.3
16196	2014-05-30T00:05:56	56807.004	67109	0.924	8.0 ± 0.4	-23.2 ± 0.4
16617	2014-05-31T01:27:04	56808.060	58860	0.749	7.3 ± 0.4	-22.2 ± 0.4
16616	2014-06-03T22:26:17	56811.935	34530	0.953	6.7 ± 0.5	-18.4 ± 0.2
16197	2014-06-06T12:32:26	56814.523	67790	0.735	7.5 ± 0.4	-15.7 ± 0.4
16198	2014-06-11T20:20:49	56819.848	39465	0.688	9.0 ± 0.6	-10.5 ± 0.2
16621	2014-06-14T14:46:41	56822.616	44400	0.758	8.4 ± 0.5	-7.7 ± 0.3
16200	2014-06-26T20:01:47	56834.835	27361	0.557	9.7 ± 0.9	$+4.4 \pm 0.2$
16201	2014-07-21T22:13:45	56859.926	58390	0.894	7.0 ± 0.4	$+29.7 \pm 0.4$
16640	2014-07-24T11:21:26	56862.473	61679	0.789	6.6 ± 0.4	$+32.3 \pm 0.4$
16202	2014-08-19T15:30:01	56888.646	65128	0.935	4.3 ± 0.3	$+58.5 \pm 0.4$
17312	2014-08-22T06:21:18	56891.265	44895	0.939	3.8 ± 0.3	$+61.0 \pm 0.3$
16203	2014-09-02T12:47:11	56902.533	41423	0.946	4.5 ± 0.4	$+72.2 \pm 0.3$
17413	2014-09-08T15:21:28	56908.640	24650	0.931	3.9 ± 0.5	$+78.2 \pm 0.2$
17414	2014-09-13T12:24:59	56913.517	17317	0.942	3.2 ± 0.5	$+83.0 \pm 0.1$
16442	2014-10-25T13:38:44	56955.569	48350	0.943	2.8 ± 0.3	$+125.3 \pm 0.3$
17545	2014-10-28T04:14:57	56958.177	34530	0.941	3.0 ± 0.3	$+127.8 \pm 0.2$
5906	2006-01-21T19:04:02	53756.794	12317	0.997	2.8 ± 0.6	$+132.0 \pm 0.1$
17544	2014-11-01T16:52:08	56962.703	25642	0.942	2.8 ± 0.4	$+132.3 \pm 0.2$
7263	2006-01-22T16:51:51	53757.703	42528	0.997	3.2 ± 0.3	$+133.1 \pm 0.3$
7264	2006-01-30T15:06:27	53765.629	37593	1.000	3.2 ± 0.3	$+141.0 \pm 0.2$
16443	2014-11-14T23:14:31	56975.968	34530	0.944	2.3 ± 0.3	$+145.6 \pm 0.2$
17486	2014-12-04T13:39:50	56995.569	33541	0.941	2.3 ± 0.3	$+165.2 \pm 0.2$
17555	2014-12-06T16:40:37	56997.695	55247	0.945	2.7 ± 0.3	$+167.4 \pm 0.3$
17561	2014-12-20T17:22:40	57011.724	54567	0.945	2.5 ± 0.2	$+181.5 \pm 0.3$
17562	2014-12-25T15:11:01	57016.633	42031	0.946	2.2 ± 0.3	$+186.3 \pm 0.3$
16444	2014-12-27T22:58:58	57018.958	41440	0.942	2.7 ± 0.3	$+188.6 \pm 0.3$
16448	2015-02-14T11:54:08	57067.496	34599	0.943	2.5 ± 0.3	$+237.1 \pm 0.2$
17602	2015-02-19T13:57:46	57072.582	51705	0.944	2.4 ± 0.2	$+242.3 \pm 0.3$
16447	2015-03-26T05:26:59	57107.227	26868	0.944	1.9 ± 0.3	$+276.8 \pm 0.2$
16199	2015-03-27T20:27:05	57108.852	39461	0.943	2.2 ± 0.3	$+278.5 \pm 0.2$
17640	2015-03-31T13:14:43	57112.552	26318	0.941	2.3 ± 0.4	$+282.1 \pm 0.2$
17641	2015-04-04T19:45:40	57116.823	24638	0.939	2.2 ± 0.4	$+286.4 \pm 0.2$